Li–Air Rechargeable Battery Based on Metal-free Graphene Nanosheet Catalysts

Eunjoo Yoo and Haoshen Zhou*

Energy Technology Research Institute, National Institute of Advanced Industrial Science and Technology, Umezono 1-1-1, Central 2, Tsukuba, Ibaraki 305-8568, Japan

ABSTRACT Metal-free graphene nanosheets (GNSs) were examined for use as air electrodes in a Li–air battery with a hybrid electrolyte. At 0.5 mA cm^{-1}, the GNSs showed a high discharge voltage that was near that of the 20 wt % Pt/carbon black. This was ascribed to the presence of sp^3 bonding associated with edge and defect sites in GNSs. Moreover, heat-treated GNSs not only provided a similar catalytic activity in reducing oxygen in the air, but also showed a much more-stable cycling performance than GNSs when used in a rechargeable Li-air battery. This improvement resulted from removal of adsorbed functional groups and from crystallization of the GNS surface into a graphitic structure on heat treatment.

KEYWORDS: graphene nanosheets (GNSs) · air-electrode · discharge overpotential · hybrid electrolyte · Li–air battery

Although rechargeable lithium-ion batteries are widely used in mobile phones, laptop computers, and similar electronic devices, their energy density is still insufficient to permit their use in electric vehicles. Recently, however, Li–air batteries have shown promise as candidates for use as high-energy-density batteries, but they still suffer from one serious problem, in that the solid reaction product (Li_2O or Li_2O_2) is insoluble in organic electrolytes.[1–3]

Our group has reported the development of a new type of Li–air battery with a hybrid electrolyte designed to overcome the problem of conventional Li–air batteries.[4] In the new battery, an organic electrolyte is used on the anode (metallic lithium) side, and an aqueous electrolyte is used on the cathode (air) side. The two electrolytes are separated from one another by a solid-state electrolyte [a lithium superion-conductor glass film (LISICON)] so that they do not intermix. However, several problems remain to be overcome, such as the complex cell structure, the stability of the LISICON, and corrosion of the air electrode catalysts. Corrosion of the air electrode catalysts is considered to result from oxidation of carbon to form Li_2CO_3. It is therefore important to choose suitable electrode materials to improve the performance of the battery.

In general, the air electrode for a Li–air battery is prepared from a combination of Pt–Au or a metal oxide such as Mn_3O_4 supported on a carbon material.[3–5] In almost all cases, mesoporous carbon has been used as the support for the metal nanoparticles. Such mesoporous carbon-supported electrocatalysts have shown quite moderate performance in Li–air batteries, and several major obstacles arising from the carbonaceous air cathode, such as carbon's oxidation in both charge and discharge processes, remain to be overcome if the cycling efficiency and cycle life of Li–air batteries are to be improved.

Recently, graphene nanosheets (GNSs), which have a two-dimensional carbon nanostructure, have attracted a great attention as a carbon support material for electrocatalysts, energy-storage materials, and polymer composites.[6–10] This is because GNSs have a high thermal conductivity (~5000 $W \cdot m^{-1} \cdot K^{-1}$), a high electrical conductivity (10^3–10^4 Sm^{-1}), and a high specific surface area (calculated theoretical value 2630 $m^2 \cdot g^{-1}$).[11,12] GNSs have been prepared by a chemical method that readily produces exfoliated graphene sheets from graphite on a large-scale. The products have many edge sites and defect sites located on the GNSs surface. Such edge and defect sites are considered to serve as active sites for chemical reactions. Furthermore, the two-dimensional structure of GNSs provides a pathway for access by oxygen gas from both sides of the nanosheet. With these characteristics, GNSs were expected to be useful novel catalysts for Li–air batteries. However, until now, although GNSs have been widely investigated as support hosts for catalysts, metal-free GNSs have not been

* Address correspondence to hs.zhou@aist.go.jp.

Received for review January 8, 2011 and accepted March 11, 2011.

Published online March 25, 2011
10.1021/nn200084u

directly used as catalysts in air electrodes for either fuel cells or Li−air batteries.

In this study, GNSs and heat-treated GNSs were prepared by a chemical method, and their electrochemical properties as air−electrode catalysts for new type of Li−air battery were studied, with particular attention to their charge−discharge performance.

RESULT AND DISCUSSION

The surface area of GNSs was 342.6 $m^2 \cdot g^{-1}$, as measured by the BET method; the surface areas of the heat-treated GNSs and AB used in this study were 211.1 and 74.9 $m^2 \cdot g^{-1}$, respectively.

Figure 1 shows the structure of the rechargeable Li−air battery based on GNSs as an air electrode. The GNS is a two-dimensional surface composed of strongly bonded carbon atoms and it has a high electronic conductivity as well as a high surface area. The surface of the GNS contained many edge and defect sites, such as carbon vacancies and five- or seven-membered rings. These edge and defect sites can effectively serve as active sites for specific chemical reactions; for example, they can act as catalysts for reduction of oxygen because, in comparison with the stacked structure of graphite, the two-dimensional structure of GNSs permits ready access of oxygen gas from both sides of the nanosheet onto defect sites and edges. The expected reaction pathway for the air electrode is shown in Figure 1. The edge or defect sites, which are attributed to sp^3 bonding of the GNS surfaces, dissociate O_2 into atomic oxygen that then migrates to the GNS surface and forms hydroxide ions (OH^-) by reaction with H_2O molecules in the aqueous electrolyte.

Figure 2a shows the discharge curves for Li−air batteries based on GNS, AB, or 20 wt % Pt/CB catalysts at a current density of 0.5 $mA \cdot cm^{-2}$ for 24 h at room temperature. The discharge voltage was a constant 3.05, 3.00, or 2.78 V *versus* Li/Li^+ for 20 wt % Pt/CB, GNSs, and AB, respectively. Interestingly, the discharge voltage of GNSs is near that of 20 wt % Pt/CB, indicating that the metal-free GNSs exhibited a high catalytic activity as a cathode electrode in the Li−air battery. However, for AB, the discharge voltage was 0.28 V less than that of 20 wt % Pt/CB. The significant difference in the catalytic activities of Li−air battery electrodes based on GNSs and AB must be due to differences in the carbon materials. We therefore considered that metal-free GNSs might be a promising candidate for use in an air electrode for a new type of Li−air battery. Figure 2b shows the charge−discharge curves for GNSs at a current density of 0.5 $mA \cdot cm^{-2}$ for 1-50 cycles. The difference between the charge voltage and the discharge voltage is denoted here as the voltage gap. The

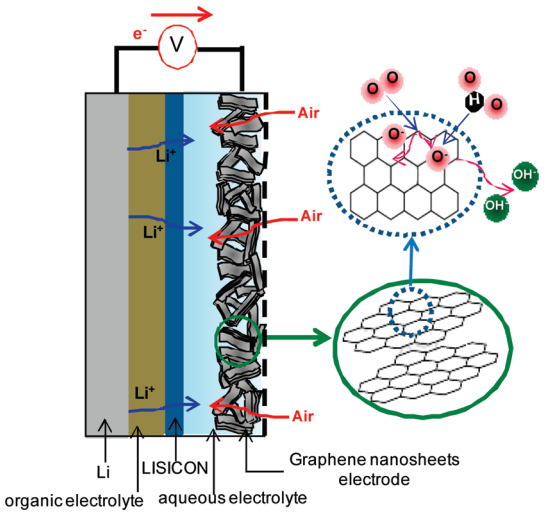

Figure 1. Structure of the rechargeable Li−air battery based on GNSs as an air electrode.

voltage gap at the first cycle was approximately 0.56 V, which was much lower than the reported values for Li−air batteries (1.0 and 0.7 V).[5,14] However, with increasing numbers of charge−discharge cycles, the charge voltage increased from about 3.55 to 3.98 V after the 50th cycle. The discharge voltage also decreased from 3.0 to 2.78 V after the 50th cycle. The voltage gap at the 50th cycle was about 1.20 V. The enhanced voltage gap probably arises from the presence of many carbon vacancies and defects on the GNSs surface, those are formed as a result of the preparation of the GNSs by chemical reduction of exfoliated graphite oxide sheets.[15] These vacancies and defects might promote corrosion of the GNSs during the electrochemical reduction of O_2 from the air. Figure 2 panels c and d show the charge−discharge curves from the first cycle to the 50th cycle for Li−air batteries with GNSs and heat-treated GNSs as catalysts, respectively, at a current density of 0.5 $mA \cdot cm^{-2}$ with charge and discharge for 2 h each. For the GNSs, the charge voltage gradually increased and the discharge voltage gradually decreased with each cycle. The difference in the discharge voltage between the first and the 50th cycle was only 0.2 V. However, the difference in the charge voltage between the first and the 50th cycle was as high as 0.4 V. This shows that corrosion in the charge process is much more serious than that in discharge process, possibly as a result of oxidation of the GNSs by the oxygen atoms released in the charge process.

In the case of heat-treated GNSs, however, neither the charge voltage nor the discharge voltage showed a significant difference after as many as 50 cycles. The difference in the charge voltage between the first and the 50th cycle was only 0.16 V. This showed that heat-treated GNSs are much more stable and cannot be easily oxidized by the oxygen atoms released in the charge process. Moreover, the

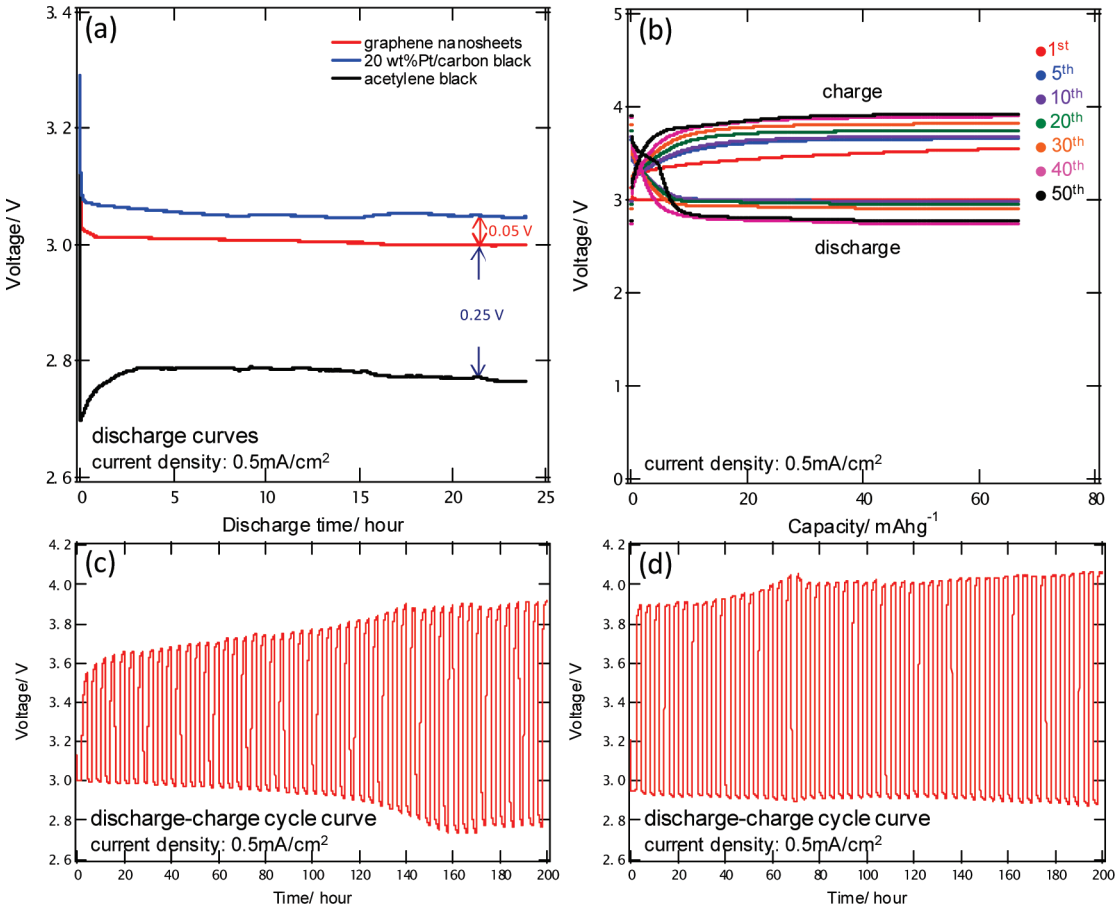

Figure 2. Discharge curves of 20 wt % Pt/CB, GNSs, and AB at a current density of 0.5 mA·cm^{-2} for 24 h (a), the correlation between cycle number and capacity of GNSs (b). Charge−discharge curves of GNSs (c) and heat-treated GNSs (d) at a current density of 0.5 mA·cm^{-2} from 1 to 50 cycles.

difference in the discharge voltage between the first and the 50th cycle was as little as 0.07 V. Thus, the improved charge−discharge cycling performance suggests that heat-treated GNSs have a good durability when used in Li−air rechargeable batteries. The improvement may be the result of changes in the surface structure of GNSs on heating. The high durability of heat-treated GNSs is ascribed to the restoration of the carbon framework, as suggested by the high quality of graphitization of the surface carbon, as confirmed by X-ray photoelectron spectroscopy (XPS) and discussed in detail below.

Figure 3 shows the discharge curves at various current densities, which provide information on the internal resistances of the cells. The operating voltage of the Li−air battery remained at 3.17 V at a current density of 0.01 mA·cm^{-2}, whereas it still remained at 2.3 V even though at a current density of 3 mA·cm^{-2}. On increasing the current density, the operating voltage linearly decreased, as can be clearly observed in the inset to Figure 3; this is mainly due to the resistance of the LISICON. By analyzing the current−voltage curve shown in the inset to Figure 3, we estimated the

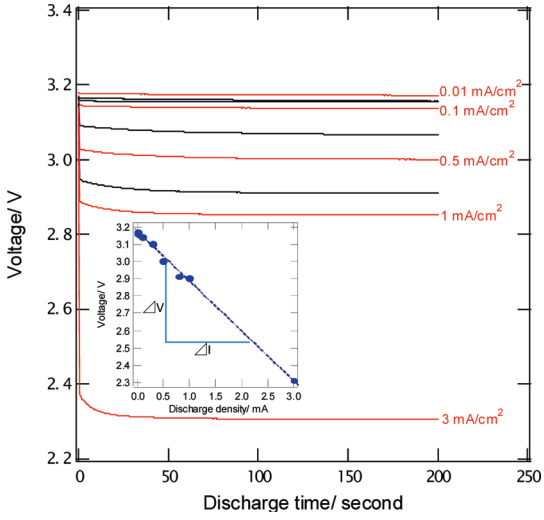

Figure 3. Discharge curves of GNSs at different current densities, from 0.01 mA·cm^{-2} to 3 mA·cm^{-2}. The inset is the *I*−*V* curve of GNSs.

internal resistance of this Li−air battery system to be about 200 Ω.

Figure 4 shows the discharge overpotential of all the measured samples, obtained from Figure 1c,d. The

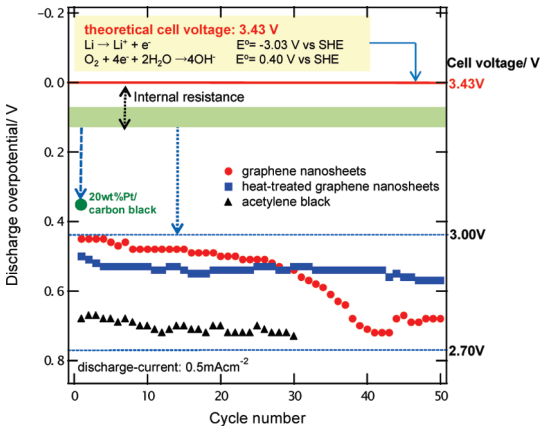

Figure 4. Discharge overpotential of all measured sample. The discharge overpotential was estimated from Figure 1c, d, asuming the internal resistance due to LISCON is 0.1 V.

following reaction occurs at the lithium anode in the Li−air battery:

Discharge:

$$Li \rightarrow Li^+ + e^- \qquad E^\circ = -3.03\ V\ versus\ SHE \qquad (1)$$

Charge:

$$Li^+ + e^- \rightarrow Li \qquad E^\circ = -3.03\ V\ versus\ SHE \qquad (2)$$

Here, SHE is the standard hydrogen electrode. At the air cathode, oxygen and water are reduced to form hydroxide ions (OH^-), in the discharge process, as shown in eq 3. In a basic electrolyte, a direct four-electron reaction occurs as follows:

Discharge:

$$O_2(g) + 4e^- + 2H_2O \rightarrow 4OH^-(aq)$$
$$E^\circ = 0.40\ V\ versus\ SHE \qquad (3)$$

Charge:

$$4OH^-(aq) \rightarrow O_2(g) + 2H_2O + 4e^-$$
$$E^\circ = 0.40\ V\ versus\ SHE \qquad (4)$$

The theoretical cell voltage is therefore 3.43 V. The discharge potential loss from internal resistance in this system is estimated assuming internal resistance of 0.1 V, because the internal resistance of LiSICON is estimated to be 200 Ω (Figure 3) and the electrochemical test is carried out at a current density of 0.5 mA cm^{-1}. Here, the discharge overpotential is defined as $\Delta V_x = V_0 - V_{xdis} - 0.1$ V, where V_0 is the theoretical cell voltage, V_{xdis} is the discharge voltage at each cycle x, and 0.1 V is the internal resistance factor. The difference in the discharge overpotential between the first cycle and the 50th cycle is denoted as ΔG. The value of ΔV_1 for 20 wt % Pt/CB was about 0.25 V, showing that it has the best performance of any cathode among the measured samples. The values of ΔV_1 were about 0.35, 0.4, and 0.58 V for GNSs, heat-treated GNSs, and AB, respectively. However, after 50 cycles, a significant difference was observed in the values of ΔG. GNSs showed a ΔV_{50} of ~0.7 V, whereas heat-treated GNSs showed a ΔV_{50} of 0.47 V. In comparison, the value of ΔG for GNSs was 0.35 V and that for heat-treated GNSs was as little as 0.07 V, which shows an excellent charge−discharge cycle performance for the Li−air battery. It was thus considered that the durability in the electrochemical test is markedly dependent on the thermal treatment of the GNSs.

The morphological structures of GNSs and AB were examined by TEM. Figure 5 shows TEM images of GNSs and AB. As can be seen in Figure 4a, the GNSs have a curled morphology with a thin, wrinkled, paper-like structure. To elucidate its atomic structure and layer stacking, we examined the GNSs by high-resolution TEM (HRTEM). A graphite hexagonal lattice could be seen in the HRTEM image. TEM imaging next to the edge confirms that the GNSs consisted of one- and two-layer graphene sheets, seen as two sets of dark lines running in a parallel direction [Figure 5b]. Furthermore, the electron-diffraction pattern was recorded to confirm the structure of GNSs [inset to Figure 5b]. The well-defined 6-fold-symmetry diffraction pattern was similar to that of peeled-off graphene, thereby confirming the crystalline structure of the as-prepared GNSs.[16] The fact that the {2110} spots appear to be more intense than the {1100} spots provides further confirmation that the resulting graphene consisted of several layer sheets.[17] Thus, the electron-diffraction pattern seen in the inset of Figure 5b demonstrates the presence of a graphene sheet consisting of a few layers. Furthermore, Figure 5c shows a conventional TEM image of AB in which the particles can be seen to have an aggregated structure of nanoparticles linked to one another to form a linear chain-like structure.

XPS was used to estimate the number of defects in the GNSs. Figure 6a shows the C_{1s} XPS spectra of GNSs and heat-treated GNSs. The curves are deconvoluted into three or four peaks, depending on the sample. In brief, the spectra clearly show the presence of a considerable degree of oxidation, with four components that correspond to carbon atoms in various functional groups, including nonoxygenated ring C═C sp^2 bonding at 284.6 eV, sp^3 bonding at 285.6 eV, carbonyl carbon (C═O) at 286.8 eV, and carboxylate carbon (O−C═O) at 288.4 eV.[18,19] Although the C_{1s} XPS spectra of heat-treated GNSs also show these same functionalities, the intensities of the corresponding peaks are much smaller than those in GNSs. In addition, as can be seen in Figure 6b, the O_{1s} XPS spectra of heat-treated GNSs also show that their peak intensity is much less than that of GNSs. On the basis of these results, we conclude that heat-treatment of GNSs promotes the removal of functional groups from the GNSs. This result is in agreement with results of thermogravimetry (TG) and differential thermal analysis (DTA) (see Supporting Information, Figure S2). Figure 6c

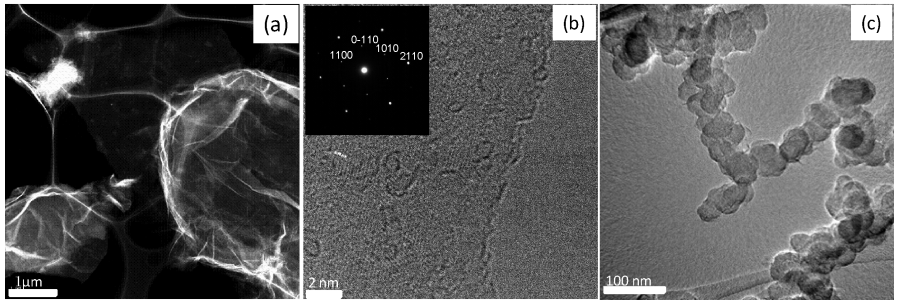

Figure 5. TEM images of GNSs (a) and AB (c). The HRTEM image of GNSs (b).

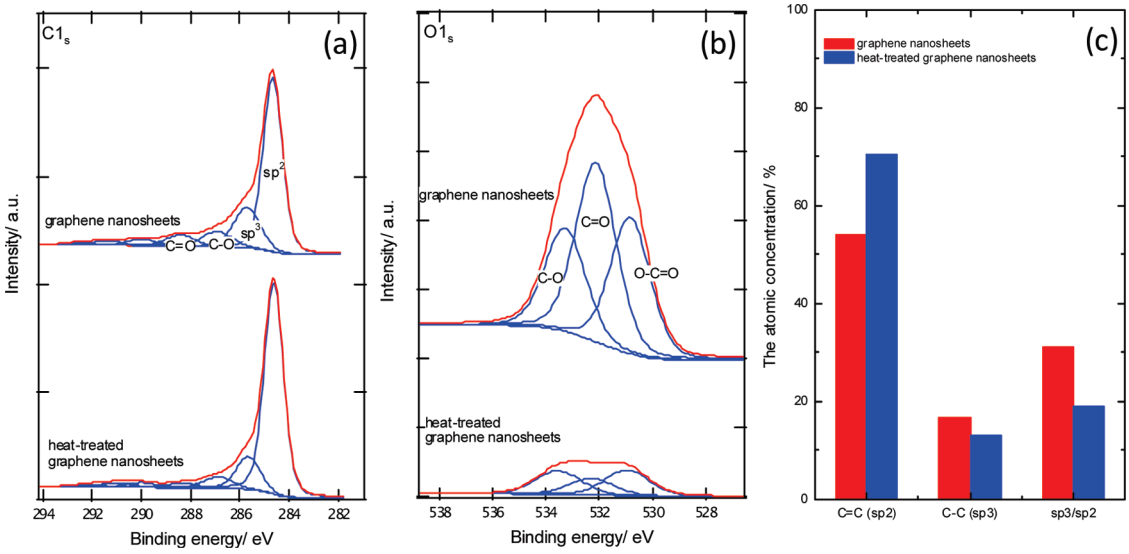

Figure 6. XPS spectra of (a) C_{1s} and (b) O_{1s} for GNSs and heat-treated GNSs. The atomic concentration by integrating XPS peak of sp^2 bonding, sp^3 bonding, and sp^3/sp^2 ratio for GNSs and heat-treated GNSs (c).

shows the contents of the various functional groups on GNSs and heat-treated GNSs, calculated by integrating the corresponding XPS peaks. The sp^3 and sp^2 carbon contents, attributed to diamond and graphite, respectively, were obtained by integrating the corresponding component against the binding energy. The relative content of sp^2 carbon in defect-free graphite for GNSs is 54.1%, which is much less than that in the heat-treated GNSs (70.3%). On the other hand, the percentage of sp^3 bonding associated with defect carbons in GNSs is higher (16.6%) than that in the heat-treated GNSs (13.2%). We also investigated the sp^3/sp^2 hybridization ratios of GNSs and of heat-treated GNSs to understand the dependence of defects and edges state on GNSs for electrochemical performance. The sp^3/sp^2 hybridization ratio was derived from their relative contents. After heat treatment of GNSs, the carbon sp^3/sp^2 hybridization ratio decreased from 31% to 19%, indicating that the sp^2 bond is more thermally stable than the sp^3 bond. The decrease in the sp^3/sp^2 ratio is mainly caused by an increase of sp^2-bonded carbon sites due to the formation of graphitized C−C bonds on heating. We confirmed the graphit ization of GNSs after heat-treatment by means of Raman spectroscopy (Supporting Information, Figure S3). The ratio of the intensities of the G and D bands (I_G/I_D), assigned to the active E_{2g} vibrations of graphite and disordered structures, respectively, was 0.54 for GNS and 0.72 for heat-treated GNSs, indicating that the GNSs was graphitized on annealing.

Jiang *et al*. have reported that the zigzag edge of a graphene nanoribbon has a unique electronic state, and that this might serve as an active site for specific chemical reactions.[20] In other words, sp^3-bonded carbon atoms in GNSs, the presence of which is attributed to edge states and defects, might serve as active sites for the oxygen-reduction reaction in the basic electrolyte of the Li−air battery, so that GNSs exhibit a high electrochemical performance in the Li−air battery.

We have therefore demonstrated that metal-free GNSs shows a good performance as a catalyst for reducing oxygen in the air in Li−air batteries with a hybrid electrolyte, even though it shows a little poor cycling performance. The low overpotential of GNSs used in Li−air battery derives from both the presence of dangling σ-bonds (sp^3 carbon atoms) at the edges and defects of GNSs.[21] The higher electronic

conductivity of GNSs also contributes to the low overpotential of GNSs used in Li-air battery. Moreover, heat-treated GNSs show a much more-stable cycling performance. Two possible reasons for the improved cycle stability are proposed on the basis of the surface state of heat-treated GNSs. The first is a decrease in the sp^3/sp^2 ratio as a result of crystallization of the GNSs surface on heat treatment. The second is that removal of functional groups from the GNSs surface by heat treatment prevents oxidation by the oxygen atoms released in the charging process. Although the detailed mechanism for the oxygen-reduction reaction on GNSs without metal is unclear, it has been shown that the GNSs are expected to be good catalysts for cathode electrode of Li−air batteries.

MATERIALS AND METHODS

GNSs were obtained by using precursor graphite as a starting material through the chemical reduction of graphite oxide in solution.[13,15] Graphite oxide was reduced by stirring with hydrazine hydrate at room temperature for 24 h, washed with distilled water until neutral, and then dried at room temperature for 24 h to obtain the GNSs. To graphitize the surface of the GNSs, it was heated in a quartz-tube reactor in flowing 4% H_2/Ar (50 cm^3/min) for 30 min at 950 °C.

Catalyst pastes were prepared from GNSs, heat-treated GNSs, or acetylene black (AB) by the following procedure. The carbon material (GNSs, heat-treated GNSs, or AB) (90%), poly(tetrafluoroethylene) (PTFE) (7%) and AB (3%) were well mixed, and the mixture was then roller-pressed into a sheet to form the catalytic layer. A gas-diffusion layer was prepared by mixing the carbon material (GNSs, heat-treated GNSs, or AB,) (60%) with PTFE (40%), and then rolling the mixture to form a film. Finally, the air catalytic layer was prepared by pressing the catalytic layer and the gas-diffusion layer onto a nickel foam.

The electrochemical test set up used for the Li−air battery with a hybrid electrolyte has been described in a previous report from our group.[4] 1 M $LiClO_4$/ED/DEC was used as the organic electrolyte, and 1 M $LiNO_3$ + 0.5 M LiOH was used as the aqueous electrolyte. A solid-state electrolyte $Li_{1+x+y}Al_x(Ti,Ge)_{2-x}Si_yP_{3-y}O_{12}$ (LISICON) film was used as a separating membrane between the organic and aqueous electrolytes to prevent intermixing of the two solutions. The cells were discharged at a current density of 0.5 $mA \cdot cm^{-2}$ for 24 h. The charge−discharge performance was carried out the voltage range 2−4.8 V at a current density of 0.5 $mA \cdot cm^{-2}$ for 2 h.

The GNSs, heat-treated GNSs, and AB were characterized by means of X-ray photoelectron spectroscopy (XPS) (S-Probe ESCA model 2803) and transmission electron microscopy (TEM) (JEOL, JEM-2010F). The Brunauer−Emmet−Teller (BET) specific surface areas were measured by means of N_2 adsorption by using a Micromeritics TriStar instrument.

Commercial 20 wt % Pt/carbon black (CB) (Johnson Matthey) and AB were used as reference materials under the same experimental conditions to compare the performance of the electrodes in the Li−air battery.

Acknowledgment. LISICON (lithium superion conductor glass film) was provided by the Ohara Company in Japan. We thank J. D. Kim of MINS Tsukuba for performing the TEM measurements, and Y. G. Wang and P. He of AIST Tsukuba for their helpful discussions and suggestions.

Supporting Information Available: The atomic concentration of C_{1s} and O_{1s} peak obtained from XPS analysis; TG and TDA of GNSs, heat-treated GNSs, GO, and AB; discharge voltage of the heat-treated GNSs and the correlation between cycle number and capacity of heat-treated GNSs; Raman spectra of GNSs and heat-treated GNSs. This material is available free of charge *via* the Internet at http://pubs.acs.org

REFERENCES AND NOTES

1. Abraham, K. M.; Jiang, Z. A Polymer Electrolyte-Based Rechargeable Lithium/Oxygen Battery. *J. Electrochem. Soc.* **1996,** *143*, 1–5.
2. Ogasawara, T.; Débart, A.; Holzapfel, M.; Novák, P.; G. Bruce, P. G. Rechargeable Li_2O_2 Electrode for Lithium Batteries. *J. Am. Chem. Soc.* **2006,** *128*, 1390–1393.
3. Debart, A.; Paterson, A. J.; Bao, J.; Bruce, P. G. A-MnO_2 Nanowires: A Catalyst for the O_2 Electrode in Rechargeable Lithium Batteries. *Angew. Chem., Int. Ed.* **2008,** *47*, 4521–4524.
4. Wang, Y.; Zhou, H. A Lithium−Air Battery with a Potential to Continuously Reduce O_2 from Air for Delivering Energy. *J. Power Sources* **2010,** *195*, 358–361.
5. Lu, Y. C.; Xu, Z.; Gasteiger, H. A.; Chen, S.; Hamad-Schifferli, K.; Yang, S. H. Platium-Gold Nanoparticles: A Highly Active Bifunctional Electrocatalyst for Rechargeable Lithium−Air Batteries. *J. Am. Chem. Soc.* **2010,** *132*, 12170–12171.
6. Stankovich, S.; Dikin, D. A.; Dommett, Geoffrey H. B.; Kohlhaas, K. M.; Zimney, E. J.; Stach, E. A.; Piner, R. D.; Nguyen, S. T.; Ruoff, R. S. Graphene-Based Composite Materials. *Nature* **2006,** *442*, 282–286.
7. Ramanathan, T.; Abdala, A. A.; Stankovich, S.; Dikin, D. A.; Herrera-Alonso, M.; Piner, R. D.; Adamson, D. H.; Schniepp, H. C.; Chen, X.; Brinson, L. C..; *et al.*Functionalized Graphene Sheets for Polymer Nanocomposites. *Nat. Nanotechnol.* **2008,** *3*, 327–331.
8. Yoo, E. J.; Kim, J.; Hosono, E.; Zhou, H. S.; Kudo, T.; Honma, I. Large Reversible Li Storage of Graphene Nanosheet Families for Use in Rechargeable Lithium Ion Batteries. *Nano Lett.* **2008,** *8*, 2277–2282.
9. Paek, S. M.; Yoo, E. J.; Honma, I. Enhanced Cycle Performance and Lithium Storage Capacity of SnO/Graphene Nanoporous Electrodes with Three-Dimensionally Delaminated Flexible Structure. *Nano Lett.* **2009,** *9*, 72–75.
10. Seger, B.; Kamat, P. V. Electrocatalytically Active Graphene−Platinum Nanocomposites. Role of 2-D Carbon Support in PEM Fuel Cells. *J. Phys Chem. C* **2009,** *113*, 7990–7995.
11. Balandin, A. A.; Ghosh, S.; Bao, W.; Calizo, I.; Teweldebrhan, D.; Miao, F.; Lau, C. N. Superior Thermal Conductivity of Single-Layers Graphene. *Nano Lett.* **2008,** *8*, 902–907.
12. Stoller, M. D.; Park, S.; Zhu, Y.; An, J.; Ruoff, R. S. Graphene-Based Ultracapacitors. *Nano Lett.* **2008,** *8*, 3498–3502.
13. Hummers, W. S.; Offeman, R. J. Preparation of Graphitic Oxide. *J. Am. Chem. Soc.* **1958,** *80*, 1339.
14. Zhou, H.; Wang, Y.; Li, H.; He, P. The Development of a New Type of Rechargeable Batteries Based on Hybrid Electrolytes. *ChemSusChem.* **2010,** *3*, 1009–1019.
15. Yoo, E. J.; Okata, T.; Akita, T.; Kohyama, M.; Nakamura, J.; Honma, I. Enhanced Electrocatalytic Activity of Pt Subnanoclusteres on Graphene Nanosheet Surface. *Nano Lett.* **2009,** *9*, 2255–2259.
16. Meyer, J. C.; Geim, A. K.; Katsnelson, M. I.; Novoselov, K. S.; Booth, T. J.; Roth, S. The Structure of Suspended Graphene Sheets. *Nature* **2007,** *446*, 60–63.
17. Hernandez, Y.; Nicolosi, V.; Lotya, M.; Blighe, F. M.; Sun, Z.; De, S.; McGovern, I. T.; Holland, B.; Gun'Ko, Y. K.; Coleman, J. N..; *et al.*High-Yield Production of Graphene by Liquid-Phase Exfoliation of Graphite. *Nat. Nanotechnol.* **2008,** *3*, 563–568.
18. Jin, M.; Jeong, H. K.; Kim, T. H.; So, K. P.; Cui, Y.; Yu, W. J.; Ra, E. J.; Lee, Y. H. Synthesis and Systematic Characterization

of Functionalized Graphene Sheets Generated by Thermal Exfoliation at Low Temperature. *J. Phys. D: Appl. Phys.* **2010,** *43*, 275402–275408.
19. Zu, S. Z.; Han, B. H. Aqueous Dispersion of Graphene Sheets Stabilized by Pluronic Copolymers: Formation of Supramolecular Hydrogel. *J. Phys. Chem. C* **2009,** *113*, 13651–13657.
20. Jiang, B.; Sumpter, B. G.; Dai, S. Unique Chemical Reactivity of a Graphene Nanoribbon's Zigzag Edge. *J. Chem. Phys.* **2007,** *126*, 134701-1–134701-6.
21. Kondo, T.; Iwasaki, Y.; Honma, Y.; Takagi, Y.; Okada, S.; Nakamura, J. Formation of Nonbonding π Electronic State of Graphite Due to Pt−C Hybridization. *Phys. Rev. B* **2009,** 233408.